Hydrol. Earth Syst. Sci. Discuss., 9, 1547–1587, 2012
www.hydrol-earth-syst-sci-discuss.net/9/1547/2012/
doi:10.5194/hessd-9-1547-2012

Hydrology and Earth System Sciences Discussions

Combining surface reanalysis and remote sensing data for monitoring evapotranspiration

M. Marshall[1], K. Tu[2], C. Funk[1], J. Michaelsen[1], P. Williams[1], C. Williams[3], J. Ardö[4], B. Marie[5], B. Cappelaere[5], A. Grandcourt[6,7], A. Nickless[8], Y. Nouvellon[6,7], R. Scholes[8], and W. Kutsch[9]

[1]Department of Geography, Climate Hazards Group, UC Santa Barbara, Santa Barbara, CA, USA
[2]Department of Integrative Biology, 4007 VLSB, UC Berkeley, Berkeley, CA, USA
[3]Department of Geography, Clark University, Worcester, MA, USA
[4]Department of Earth and Ecosystem Sciences, Division of Physical Geography and Ecosystem Analysis, Lund University, Sölvegatan 12, 223 62 Lund, Sweden
[5]Institut de recherche pour le développement, UMR HydroSciences, BP 64501, 34394 Montpellier cx 5, France
[6]CIRAD, Persyst, UPR80, 34398 Montpellier Cedex 5, France

[7]CRDPI, BP 1291, Pointe-Noire, Republic of Congo
[8]Natural Resources and the Environment, Council of Scientific and Industrial Research, Pretoria, South Africa
[9]Johann Heinrich von Thünen-Institute, Institute for Agricultural Climate Research, Bundesallee 50, 38116 Braunschweig, Germany

Received: 14 December 2011 – Accepted: 4 January 2012 – Published: 2 February 2012

Correspondence to: M. Marshall (marshall@geog.ucsb.edu)

Published by Copernicus Publications on behalf of the European Geosciences Union.

Abstract

Climate change is expected to have the greatest impact on the world's poor. In the Sahel, a climatically sensitive region where rain-fed agriculture is the primary livelihood, expected decreases in water supply will increase food insecurity. Studies on climate change and the intensification of the water cycle in sub-Saharan Africa are few. This is due in part to poor calibration of modeled actual evapotranspiration (AET), a key input in continental-scale hydrologic models. In this study, a model driven by dynamic canopy AET was combined with the Global Land Data Assimilation System realization of the NOAH Land Surface Model (GNOAH) wet canopy and soil AET for monitoring purposes in sub-Saharan Africa. The performance of the hybrid model was compared against AET from the GNOAH model and dynamic model using eight eddy flux towers representing major biomes of sub-Saharan Africa. The greatest improvements in model performance are at humid sites with dense vegetation, while performance at semi-arid sites is poor, but better than individual models. The reduction in errors using the hybrid model can be attributed to the integration of a dynamic vegetation component with land surface model estimates, improved model parameterization, and reduction of multiplicative effects of uncertain data.

1 Introduction

Actual evapotranspiration (AET) is the only water flux that connects the atmospheric and land water cycles (Hartmann, 1994). In semi-arid regions of Africa, AET is the dominant component of the water budget and is highly variable across vegetation types (Ramier et al., 2009). These changes can have dramatic effects on the interannual and interdecadal variability of rainfall (Zeng and Neelin, 2000). A positive land-atmosphere feedback between vegetation and rainfall, for example, has been observed in the western Sahel. A decrease in rainfall and natural vegetation, leads to an increase in surface albedo and decrease in AET, which decreases moisture input to the west African

HESSD
9, 1547–1587, 2012

monsoon circulation, thus contributing to persistent droughts there (Zeng, 2003). Understanding this important moisture flux and its relationship to rainfall is particularly important in sub-Saharan Africa, where more than 70 % of the region's livelihood is rain-fed agriculture. Near real time AET estimates modulated by regional vegetation can be a powerful tool to facilitate this endeavor.

Literature reviews of continental to global scale AET modeling techniques can be found in Diak et al. (2004), Glenn et al. (2007), and Kalma et al. (2008). For the purposes of this paper, modeling approaches can be divided into two general categories. In the first category, remote sensing derived energy flux is combined with ancillary meteorological data using simple relationships to estimate near real-time estimates of AET as a residual of the energy balance. The remaining terms in the energy balance equation (ground heat flux – G, sensible heat flux – H, and net radiation- R_N) can be determined from empirical relationships with remotely sensed surface temperature and vegetation. Remote sensing models which derive flux directly from empirical relationships of meteorological and remote sensing data are not considered in this category. Algorithms which produce global estimates of AET as a residual of the energy balance are described in Nishida et al. (2003), Leuning et al. (2008), Mu et al. (2007a), and Fisher et al. (2008). These models have been recently used in sub-Saharan Africa to estimate water use efficiency for arid rangelands (Palmer and Yanusa, 2011) and extrapolate biological nitrogen deposition from wildfires (Chen et al., 2010). One of the greatest limitations of AET estimates inferred from satellite data is that they often use once-a-day satellite overpasses and the evaporative fraction to extrapolate AET estimates over longer time scales. The evaporative fraction is the ratio of AET to R_N-G, which can be used to scale AET over the day (Mintz and Serafini, 1992). Early reports showed errors in AET using this method to be 20–40 % from surface measurements (Nichols and Cuenca, 1993). Improved satellite data and parameterization have reduced these errors, but persistent cloud cover and overestimation of net radiation due to poor cloud filtering continue to make the application of this technique difficult in the tropics.

HESSD
9, 1547–1587, 2012

The second category of models, termed Land Surface Models (LSMs), can provide near real-time, continuous and global estimates of AET using sophisticated process-based techniques driven by assimilated ground, satellite, and reanalysis data (Rodell et al., 2004). In the case of this paper, LSM's are run offline (i.e. uncoupled to the atmosphere). AET from these models is driven primarily by precipitation with latent heat being solved as a residual of the water balance and corrected using assimilated fields of the energy terms. LSM's overcome the temporal limitations associated with remote sensing based estimates of AET, because LSMs are driven by reanalysis fields of surface climate. Land surface flux has been compared from several LSM's at the global level: Project for Intercomparison of Land-Surface Parameterization Schemes (Henderson-Sellers et al., 1995), the Global Soil Wetness project (Dirmeyer et al., 2006), and a remote sensing based and LSM inter-comparison (Jiménez et al., 2011). The AMMA Land-Surface Model Inter-comparison Project (Boone et al., 2009) includes LSM comparisons in Africa in order to better understand the impact of land surface flux on the West African Monsoon. Two of the major drawbacks of LSMs is that their strong theoretical framework often makes them less robust, due to conspiring factors attributed to a multitude of data types (most importantly R_N) and empirically-based parameters (Rosero et al., 2009).

The objective of this paper is to identify and integrate components from a remote sensing based and LSM approach to improve estimates of AET. The integration of near real-time remote sensing AET models with LSM AET can help maximize the benefits of both approaches. For example, land surface temperature derived from remote sensing data are used to recalibrate AET estimates from a soil vegetation atmosphere transfer model in Olioso et al. (1999) and from a residual energy balance model in Boni et al. (2001). AET estimates in this study are improved further downstream in the modeling process by direct insertion, whereby the AET component of one model, in this case one that drives canopy AET with regular remotely sensed vegetation, is substituted with canopy AET from an LSM. The hybrid model is developed through a series of exploratory exercises, given the fundamentally different approaches each

HESSD
9, 1547–1587, 2012

model takes to estimating AET and the equally diverse strengths and weaknesses in parameterization.

The Berkeley model (Fisher et al., 2008) is selected for integration with an LSM. This model is driven primarily by vegetation controls on Rn. The Berkeley model is chosen, because it has been shown to outperform other AET models in the tropics when compared with eddy covariance flux tower data and it can be readily applied over large areas using remote sensing and surface reanalysis data. In addition, it requires no calibration (optimization) or spin-up. A major drawback to this model is that the soil and wet evaporation components are highly empirical power functions which are driven by specific humidity, a notoriously uncertain parameter in surface reanalysis datasets. Therefore, improvements in the Berkeley model can be made by further re-parameterizing wet canopy and soil evaporation. The LSM used is the NCEP, Oregon State University (OSU), Air Force, and Hydrology Research Laboratory at NWS (NOAH) model (Chen et al., 1996). NOAH is a community model which has undergone several inter-model comparisons and ground-based validations, leading to vast improvements in its parameterization since its inception at OSU. It is comparable to other LSMs when modeling latent heat flux (LE) driven by AMMA Land Surface Model Intercomparison Project forcing and parameters over large areas in western Africa (Boone et al., 2009) and generally performs better than other LSMs under semi-arid (sub-Saharan Africa) conditions (Hogue et al., 2005). The major limitation of the model is that the canopy (transpiration) component of AET is driven by long-term monthly averages of the Normalized Difference Vegetation Index (NDVI). Therefore, further improvements in NOAH AET in semi-arid regions can be made by including a dynamic vegetation component.

In the first phase of the analysis, the Berkeley model is compared with flux tower data to identify possible sources of error in model parameterization and to judge the performance of the model across various land cover types in sub-Saharan Africa. A sensitivity analysis is then performed on the model inputs to guide model re-parameterization. For example, identifying the parameters that represent a large source of model error or insensitivity would justify re-parameterization or substitution of the parameter with

HESSD
9, 1547–1587, 2012

long-term mean data. This type of exploratory analysis facilitates the development of a hybrid model, which combines the canopy component of the Berkeley model and wet canopy and soil evaporation components of the NOAH LSM. In the final phase of the analysis, the combined model is evaluated using the flux tower data.

2 Methods

2.1 The Berkeley model for actual evapotranspiration

The Berkeley model is a modified version of the original Priestley and Taylor (1972) model for potential evapotranspiration (PET). A complete description of the model and bibliography can be found in Fisher et al. (2008). The Priestley-Taylor formulation for PET reduces the advection term in the original Penman (1948) formulation to a simple coefficient (α). The Priestley-Taylor model is therefore driven primarily by net radiation and tends to perform best in humid areas and worse in moisture limited areas (DehghaniSanij et al., 2004). The Berkeley model retains the original α (1.26) and instead uses six parameters to modify PET:

$$\begin{aligned} \mathrm{LE_S} &= f_{\mathrm{SM}}(1-f_{\mathrm{WET}})(1-f_{\mathrm{C}})\frac{\alpha\Delta}{\Delta+\gamma}(R_{\mathrm{N}}-G) \\ \mathrm{LE_C} &= f_{\mathrm{C}}f_{\mathrm{G}}f_{\mathrm{T}}f_{\mathrm{M}}(1-f_{\mathrm{WET}})\frac{\alpha\Delta}{\Delta+\gamma}(R_{\mathrm{N}}) \\ \mathrm{LE_I} &= f_{\mathrm{C}}\, f_{\mathrm{WET}}\frac{\alpha\Delta}{\Delta+\gamma}(R_{\mathrm{N}}) \end{aligned} \quad (1)$$

where f_{SM}, f_{WET}, f_{C}, f_{G}, f_{T}, and f_{M} are the soil moisture constraint, relative surface wetness, fractional total vegetation cover, green canopy fraction, plant temperature constraint, and the plant moisture constraint respectively. Table 1 lists each parameter and the relevant equation used in the computation of latent heat (LE).

The equations have been arranged to express LE in terms of its three components: bare soil evaporation ($\mathrm{LE_S}$), transpiration ($\mathrm{LE_C}$), and wet surface evaporation ($\mathrm{LE_I}$). The

HESSD
9, 1547–1587, 2012

psychometric constant (γ: 0.066 kPa °C^{-1}), slope of the saturation-to-vapor pressure curve (Δ), R_N, and G make up the Priestley-Taylor formulation for PET. Net radiation and G are readily available from surface climate reanalysis or remotely sensed spectral indices. Equation (1) is a modified version of the Fisher et al. (2008) model in which the soil and canopy contribution to $R_N$are assumed to be a function of leaf area index and f_C according to Beer's Law (Kelliher et al., 1995). Here, R_N-G is discretized by NDVI, which has been shown to be highly correlated with f_C (Sellers, 1987). Fractional total vegetation cover is expressed as a linear function of NDVI, which is determined from the red and near infrared bands of standard multi-spectral remote sensing platforms.

The transpiration component of LE has the greatest number of constraints. The green canopy fraction is a biophysical constraint expressed as the ratio of the fraction of PAR absorbed by the green vegetation (f_{APAR}) to the total amount of PAR absorbed by the canopy (f_C). Photosynthetically Active Radiation (PAR) absorbed by green vegetation is a linear function of the Enhanced Vegetation Index EVI. The Enhanced Vegetation Index is another remotely sensed spectral index and is more sensitive to the chlorophyll content of vegetation than NDVI (Gao et al., 2000). The plant temperature constraint is a physiological parameter and assumes that vegetation photosynthesizes at an accelerated rate until an optimal temperature (T_{OPT}) is achieved, after which efficiency decreases (June et al., 2004). The optimal temperature is determined over the entire available time series and is analogous to "relative greenness" in the remote sensing literature. It occurs during the primary growing season, when the daytime temperature (T_{MAX}) at which plant investment in light energy (f_{APAR}) and the availability of light (PAR) are high, and the vapor pressure deficit (VPD) is low. Surface temperature data is readily available from reanalysis data. The plant moisture constraint is the ratio of f_{APAR} to maximum f_{APAR} over the available time series. It assumes that the amount of light a plant absorbs varies with moisture availability: f_{APAR} decreases only when the plant is stressed, thus lowering transpiration when PAR is high. The effect of this constraint on LE_C is minimal, unless the plant is suffering from extreme moisture stress.

HESSD
9, 1547–1587, 2012

The interception and soil components are governed by relative humidity (RH), which can be determined from surface pressure and specific humidity reanalysis. It is assumed that bare soil evaporates water at the potential rate (PET), provided that the soil is saturated (Bouchet, 1963). When the soil is not saturated, relative humidity above the surface decreases and latent heat decreases due to lower soil water storage. The soil moisture constraint is a power function of RH and the vapor pressure deficit (VPD), which acts to reduce the supply of water to the atmosphere as the soil dries. Midday relative humidity and VPD are used, because these values show better results in the original paper than daily averages. The theoretical justification is that the coupling between soil moisture and atmospheric humidity is strongest in the daytime when vertical mixing is high. Similarly, f_{WET} is a power function of relative humidity and indicates the probability that the surface is wet; when relative humidity is 100 %, the soil and canopy are completely wetted and evaporate moisture at the potential rate.

2.2 NOAH Model for actual evapotranspiration

The earliest version of the NOAH-LSM can be traced back to Chen et al. (1996), who integrated an explicit canopy component with a simple soil water balance model developed at OSU (Pan and Mahrt, 1987). The model has undergone several revisions since that time, including improvements to bare soil evaporation estimates with the introduction of skin temperature and a dynamic soil moisture component (Betts et al., 1997) and to transpiration estimates with the introduction of a monthly fractional total vegetation cover climatology (Chen and Dudhia, 2001). The NOAH model also includes three components of latent heat. Unlike the Berkeley model, where constraints are driven primarily by changes in vegetation and atmospheric humidity, the NOAH model takes a water balance approach driven primarily by precipitation. Each energy term (LE_S, LE_C, and LE_I) is summed after constraints on PET have been computed. Potential evapotranspiration in the NOAH model (E_P) is an energy version of Penman (1948) with a detailed description in Mahrt and Ek (1984).

HESSD
9, 1547–1587, 2012

$$\mathrm{LE} = \left\{ \underbrace{(1-f_C)\beta}_{\mathrm{LE_S}} + \underbrace{B_C\left(1-\left(\frac{W_C}{S}\right)^n\right)}_{\mathrm{LE_C}} + \underbrace{f_C\left(\frac{W_C}{S}\right)^n}_{\mathrm{LE_I}} \right\} E_P \quad (2)$$

where LE (Wm^{-2}) is the latent heat flux (actual evapotranspiration), β is the fraction of total soil moisture not used by the canopy (Mahfouf and Noilhan, 1991), B_C is a function of atmospheric and stomatal resistance (Jacquemin and Noilhan, 1990), W_C is the water holding capacity of the canopy defined as the residual of water balance terms, and S is the maximum water holding capacity of the canopy (calibrated constant). As in the original Berkeley formulation, f_C is a function of LAI. It is computed from a 0.15° resolution climatology of AVHRR NDVI (Gutman and Ignatov, 1998). Soil moisture availability (β) includes a dynamic soil moisture component constrained by the wilting point and the field capacity of the soil, both of which are functions of soil texture. The constraints are elaborated upon in Table 2, while a more detailed description can be found in Chen and Dudhia (2001). The NOAH-LSM in this paper (version 2.7.1) is driven uncoupled to the atmosphere by the 0.25° resolution Global Land Data Assimilation System (GLDAS) forcing and paremeters (Rodell et al., 2004), enabled by the Land Information System (Kumar et al., 2006). Details on GLDAS forcing data can be found on NASA's Hydrology Data and Information Services Center webpage (http://disc.sci.gsfc.nasa.gov/hydrology), while details on the parameterization datasets used can be found at http://ldas.gsfc.nasa.gov/gldas/GLDASvegetation.php. Forcing data will be referred to as GLDAS for the remainder of the paper, while GNOAH will refer to NOAH-LSM output driven by GLDAS forcing and parameterization.

The hybrid model developed in this paper sums the $\mathrm{LE_I}$ and $\mathrm{LE_S}$ components from the GNOAH with $\mathrm{LE_C}$ from the Berkeley model.

HESSD
9, 1547–1587, 2012

2.3 Data processing and handling

The Berkeley model is run globally at a quasi-0.05° resolution daily time step from 2000–2008 for sub-Saharan Africa and is aggregated to a monthly time step for visualization and comparison purposes with field data. Daily values were aggregated to monthly values for several reasons: (1) ground heat flux was not calculated in the Berkeley model (ground heat flux is near zero in warm regions at a monthly time step), (2) daily station flux data was often spurious or missing, (3) the vegetation data used (see below) is extremely noisy at a daily time step and (4) dekadal to monthly timesteps are adequate to address research questions in food security monitoring and other continental scale studies.

The Global Land Data Assimilation System uses 0.25° resolution climatological forcing data for this exercise. GLDAS uses NOAA/GDAS atmospheric fields, Climate Prediction Center Merged Analysis of Precipitation fields, and observation-driven shortwave and longwave radiation using the Air Force Weather Agency's AGRicultural METeorological modeling system. These data are produced at 3-hourly intervals and aggregated to a monthly time step. The latent heat simulation from the NOAH-LSM is at 0.25° resolution and resampled using the "nearest neighbor" approach to 0.05° resolution for comparison purposes with the Berkeley model. The choice of resampling assumes that spatial heterogeneity is driven primarily by vegetation.

The NDVI and EVI 0.05° resolution vegetation index inputs come from the Moderate Resolution Imaging Spectroradiometer (MODIS) on board the Earth Observing System-Terra platform (Huete et al., 2002). The vegetation indices are composited over 16 day periods. The NDVI and EVI data are distributed by NASA with complementary information describing the reliability and quality of the data. Pixels are masked for low data reliability, aerosols, clouds, and water bodies. A piecewise weighted least squares regression filter (Swets et al., 1999) is applied to the datasets to further reduce atmospheric interference on the vegetation signal.

HESSD
9, 1547–1587, 2012

2.4 Statistical analysis

The analysis is done in three phases: (1) evaluation of the Berkeley model using station data and comparison of ground inputs with surface reanalysis data, (2) sensitivity and residual analysis of the Berkeley model, and (3) development of a combined model and inter-model comparison. The observed data are from three sources: the African Monsoon Multidisciplinary Analysis (AMMA) programme (www.amma-international.org), CarboAfrica (www.carboafrica.net) and Fluxnet (www.fluxdata.org). Table 3 lists the field sites used to estimate micro-climate and energy fluxes and includes the station I.D. and name, country, geographic coordinates, the period data is obtained, ecosystem type using the International Geosphere-Biosphere Programme (IGBP) naming convention, and climatology.

Five of the sites (BW-Ma1, CG-Euc, NE-Waf, NE-Wam, and ZA-Kru) include half-hourly measurements of surface air temperature (°C), incoming longwave and shortwave radiation ($W\,m^{-2}$), outgoing longwave and shortwave radiation ($W\,m^{-2}$), relative humidity (%), precipitation (mm), and latent heat ($W\,m^{-2}$). NE-Wam and NE-Waf were in close proximity and shared a rainfall gauge between them (Ramier et al., 2009). LE was measured using the eddy covariance method (Baldocchi et al., 1988). With this technique, latent heat flux is determined by correlating changes in water vapor concentration at the surface and at height measured using hygrometers and a sonic anemometer. The eddy covariance method is the most widely used method for measuring LE in the field. There is on average, however, a 20 % difference between measured turbulent fluxes (H and LE) and total available energy (R_N) for most sites (Wilson et al., 2002). The data used are not corrected for energy balance closure, because all three energy terms needed (R_N, H, and LE) were not available at most of the sites when the data was accessed and no universal approach for correcting this problem has been adopted. Half hourly (uncorrected) data from the flux towers are used, because the Berkeley model computes latent heat flux from daytime R_N. Average daily (corrected) data is typically filled using look-up tables (Reichstein et al., 2005) and/or artificial

HESSD
9, 1547–1587, 2012

neural networks (Papale and Valentini, 2003), however these data are not available, so persistent data gaps at some of the sites do exist.

The purpose of the first phase of the analysis is to extend comparison of the model with micrometeorological data to semi-arid zones in sub-Saharan Africa and to qualitatively assess the performance of LE parameterizations (transpiration, wet canopy evaporation, and bare soil evaporation). The comparison also helped to identify sources of error in the surface reanalysis to aid in the interpretation of the sensitivity and residual analysis. Near infrared and red reflectance are not available from the stations, so NDVI and EVI from MODIS are used to drive the local model run instead. Point to sensor scale comparison are performed by taking the average of remote sensing and surface reanalysis inputs over adjacent grid cells to the cell corresponding to the latitude and longitude of the stations. The averaging covers a footprint typically larger than that of a flux tower (<1000 m), however the averaging is deemed necessary, because many of the stations fall on the border of two or more adjacent pixels. Each component of LE is computed and compared visually with observed LE. The coefficient of determination (R^2) and root mean squared error (RMSE) are the primary metrics used for comparison of monthly Fisher LE to observed LE. It is assumed that LE_C is the largest and the primary seasonal component of LE. Wet surface evaporation is typically the smallest component and is assumed negligible. Soil evaporation tends to track well with precipitation (Nagler et al., 2007), so precipitation is used as a proxy for LE_S evaluation. Each GLDAS input (R_N, T, specific humidity – q, and surface pressure – p) is plotted against the micrometeorological data. The bias, RMSE, and correlation coefficient is calculated for each.

The purpose of the second phase of the analysis is to identify those GLDAS inputs that could potentially lead to large errors in the Berkeley model. A sensitivity analysis is used to identify which GLDAS and MODIS inputs the Berkeley model is most sensitive to. The outcome of interest in the analysis is: the model is sensitive to a particular input that is also a large source of error, necessitating calibration. Minor improvements during model calibration can also be made in the case that the input was erroneous

HESSD
9, 1547–1587, 2012

but not an important contributor to AET variability by substituting the input with the long-term mean. The residuals (observed LE minus Berkeley modeled LE) are plotted against each input variable to identify the inputs that lead to the greatest errors in modeled LE. Two cases of the sensitivity analysis are performed. In the unconditional case, all input variables (R_N, T, q, p, NDVI, and EVI) are constrained to mean values except for the test variable (Haan, 2002). The test variable is perturbed 10 000 times between $\pm 3\,\sigma$. The model output LE is regressed against the test input and the slope of the relationship is computed to determine the relative weight of each input to the output. In the conditional case, the test input or a combination of test inputs is constrained to the mean and the remaining variables are allowed to run freely. This case tests the sensitivity of the model to inputs taking into account any synergistic effects. All combinations of test inputs are evaluated by taking the ratio of the standard deviation of model output using model input(s) at their mean to the standard deviation of model output if all inputs are left free. In the residual analysis, each MODIS and GLDAS input is plotted against observed LE minus modeled LE. The correlation coefficient and significance (p-test) are used to determine the relative strength of each relationship.

The first and second phases of the analysis are used to guide the development of an LE hybrid model that combines LE components from the Fisher and GNOAH models. A time series of modeled LE using Fisher, GNOAH, and the combined model are plotted with observed LE for the eight micrometeorological stations. The coefficient of determination and RMSE between observed and modeled LE at a monthly time step are used to test the relative strength of each model and error respectively.

3 Results

3.1 Input and parameter comparison: field data

The three components (transpiration, wet canopy evaporation, and bare soil evaporation) from the Berkeley model are plotted, along with observed LE and precipitation in

HESSD
9, 1547–1587, 2012

Fig. 1. There is no surrogate for wet canopy evaporation and its low variability revealed that it is merely a background signal in total LE. The magnitude and timing of modeled LE for the five stations with sufficient data to drive the Berkeley model are captured well at three of the five sites. At the driest sites (NE-Waf and NE-Wam), the timing is captured well, but the magnitude of peak LE from the Berkeley model is less than 50 % of actual peak LE. NE-Wam was not included in the figure because the results were similar to NE-Waf. The average R^2 and RMSE across the five sites (BW-Ma1, CG-Euc, NE-Waf, NE-Wam, amd ZA-Kru) are 0.78 and 36.81 $W\,m^{-2}$, respectively. The fallow site (Ne-Waf) has the highest R^2 (0.93), reflecting the ability of the model to capture timing, but also the highest RMSE (72.47 $W\,m^{-2}$). The wooded site had the lowest R^2 (0.65). ZA-Kru had the lowest RMSE (13.75 $W\,m^{-2}$), due in part to data gaps during peak ET (wet season). During this season, sensors are frequently turned off to prevent damage from lightning and power surges.

At the driest sites, the model tends to underestimate wet season LE (peaks) and overestimate dry season LE (troughs). Latent heat from the eucalyptus plantation (CG-Euc: included in Fisher et al., 2009) is overestimated fairly consistently throughout the year. The time series at the two driest sites (NE-Wam and NE-Waf) are insufficient to discern interannual patterns, but given the sparse vegetation and lack of an advection term in the PET approach used, it is expected that the model underestimates peak latent heat for both wet and dry years. The canopy component follows the timing of total LE for all the sites, as expected, given the dominance of transpiration to total LE. Without actual transpiration data, however, it is impossible to determine the representativeness of Fisher LE_C magnitudes. Assuming a lagged relationship between soil evaporation and rainfall, LE_S performs well at the sites with low vegetation density and poorly at the sites with high vegetation density. Therefore, based on the limited field data that is available, it appears that Fisher LE_C is at least capturing the timing of observed LE well, while the Fisher LE_S parameterization tends to suffer in vegetated (humid) areas.

HESSD
9, 1547–1587, 2012

The monthly GLDAS data used to drive the Berkeley model (R_N, T_{MAX}, q, and p) are plotted against observed data for ZA-Kru in Fig. 2. It is expected that GLDAS pressure and specific humidity data correlates well with observed relative humidity. Actual specific humidity and surface pressure are not used for direct comparison, because these data are not available for most of the sites. GLDAS R_N, T, and q showed good agreement with observed data. The inverse relationship between p and relatively humidity is present, but obscured by outliers above 98.0 kPa (Fig. 2d). The outliers are from the first year of the reanalysis when the GDAS reanalysis fields are used exclusively. BW-Ma1 is the only other site that showed such a relationship. Table 4 summarizes the results for all of the stations with sufficient field data for the comparison. Some of the relationships are clearly non-linear, however statistics from a linear fit are chosen for comparison purposes between inputs and across sites. Temperature from the GLDAS dataset consistently shows high correlations across all the sites. Specific humidity is the second best predicted input. The correlation between specific humidity from the reanalysis and observed relative humidity are highest at the two driest sites (NE-Waf and NE-Wam) and lowest (negative) at the most humid site (CG-Euc), which could be due to the low variability in relative humidity and relatively larger homogenous area at the dry sites. GLDAS R_N was the next best predicted model input. The longest time series (CG-Euc and ZA-Kru) had the highest correlations to observed R_N, but with large biases. The longer time series and presence of outliers could therefore be inflating the correlations. In either case, the general pattern (seasonality) in R_N is being predicted well for these sites, but assuming all inputs are weighted equally, overestimates in modeled LE are likely to occur. Conversely, the weak and negative relationships between GLDAS R_N and observed R_N at the two driest sites lead to underestimates of R_N in modeled LE. Reanalysis pressure by far has the poorest correlations with observed data, as high biases are seen across all the sites.

HESSD
9, 1547–1587, 2012

3.2 Sensitivity analysis

The comparison in Sect. 3.1 revealed that Fisher LE_C performs the best of the three LE components and that GLDAS temperature, which is used exclusively in the transpiration component of the model, is the best performing input with available observed data. This exploratory exercise indicates that Fisher LE_I and LE_S may be good candidates for re-parameterization. The second phase of the analysis shows the relative contribution of inputs to model error. The results of the unconditional case of the sensitivity analysis are shown in Table 5. The results of this test are shown for ZA-Kru and are representative of the sites. The slope and intercept are generated from linear fits of model output data to input data in normalized space. The slope of the fit therefore represents the average expected increase in LE due to a standard deviation increase in the test variable. The model is most sensitive to EVI and q, because these variables have the largest slopes, while the model is least sensitive to p. Increases in NDVI and T act to suppress LE, as indicated by the negative slopes. NDVI in the Berkeley model is in the denominator of f_G, since it is used to indicate overall absorption of incoming radiation by the canopy. As NDVI increases, f_G decreases, given NDVI is more variable than EVI. Temperature is explicitly handled in the plant temperature constraint function- increases in temperature above the optimum temperature leads to increases in this constraint and lower LE. The results of the unconditional case are shown in Fig. 3. Six input variables yield sixty-two possible combinations or model realizations. The ratio of the standard deviation of the model when the test variable(s) are kept at their mean to the standard deviation of the model if all inputs are allowed to run freely represent the relative sensitivity of the model to that input or combination of inputs. The evaluation of all possible combinations reveals important synergistic effects that may enhance or suppress the predictability of LE. The various combinations are plotted against modeled LE with all inputs allowed to run freely and R is computed as well, but this chart was not included, because it did not contribute new information. Ratios less than one indicate a reduction in predictive power, while ratios greater than one reveals

HESSD
9, 1547–1587, 2012

dampening effects. As shown in Fig. 3, keeping q (input 2) and EVI (input 6) at their mean has the largest impact on modeled LE, while T (input 3) and NDVI (input 5) act to suppress modeled LE. EVI, which is used to compute the green fraction, explains nearly 60 % of the model variability alone (combination 1, 2, 3, 4, 5). Keeping NDVI and R_N at their mean (combination 4, 5) reveals no noticeable drop in modeled LE. The model inputs for EVI and q are plotted against a time series of modeled LE (not shown). EVI tends to capture the troughs in ET (dry season) when transpiration is significantly larger than soil evaporation and specific humidity is better at capturing the peaks in ET (wet season) when soil evaporation is a much larger component of the budget.

3.3 Hybrid model

The low dependence of the Berkeley model on surface pressure and spurious GNOAH pressure data suggests that minor improvements in modeled ET could be made by substituting long-term means in the GLDAS pressure data. The relatively poor parameterization of Fisher LE_S and LE_I and conflicting results of the GLDAS specific humidity data in humid areas and strong dependence of the Berkeley model on specific humidity, suggests that modest improvements in LE can be made by substituting LE_S and LE_I driven by specific humidity in the Berkeley model with a parameterization that uses a surrogate, such as precipitation or nighttime temperature. The GNOAH LE_S and LE_I components are driven primarily by precipitation, are well conceived in the literature, and therefore served as parameter substitutes in the Berkeley model. Time series of observed LE and modeled LE using Fisher, GNOAH, and the combined model (Fisher LE_C + GNOAH $LE_{I,S}$) for six of the eight stations are shown in Fig. 4. Table 6 includes goodness-of-fit statistics for six of the eight stations: ZM-Mon and NE-Wam are omitted, because the former had less than one year of data and the latter showed no noticeable difference from NE-Waf. Two of the stations (BW-Ma1 and CG-Tch) showed obvious bad (flat) LE data at the beginning and end of the time series when the sensors were just coming online or being neglected, so statistics are computed after these points were omitted. The last month of CG-Tch was omitted as well, because the site

HESSD
9, 1547–1587, 2012

was burned in July 2008, so that no grass remained until the site recovered in mid-October (data not available for the analysis). Grass was absent and the soil humidity is less than 2 % by volume, so H is the dominant energy flux.

The combined model outperforms the GNOAH model for the majority of sites and equally as well for the remaining sites. The greatest improvements are made between the Fisher and combined model, particularly in the reduction in RMSE. These improvements are greatest at the sites with dense vegetation (CG-Euc and BW-Ma1). At these sites, the combined model tends to underestimate the peaks and overestimate the troughs. At the driest sites (NE-Wam, NE-Waf, and SD-Dem), all three models grossly underestimate peak LE, however the combined model performs the best. The major limitation of GNOAH, namely lack of a dynamic vegetation component, is reflected on the time series at the ZA-Kru site. The smooth LE signal produced by the GNOAH model does not capture the natural variability of this semi-arid site. The Berkeley model represents the other extreme, as it overestimates the variability in observed LE. The combined model is a compromise between the two. All three models tend to perform poorest for CG-Tch, missing the peak in 2007 and the secondary peak in 2008.

4 Discussion

The study represents an initial attempt to use a suite of new flux tower data in sub-Saharan Africa to improve AET estimation using remote sensing and surface reanalysis data for regular near real-time continental scale monitoring. The integration of the evaporation from GNOAH with the Fisher transpiration further improves the correlations and reduces the RMSE for both humid and semi-arid sites. The fractional total vegetation cover of the GNOAH model is the single most important variable controlling transpiration. This is consistent with other findings that showed LAI was a strong control on the ratio of AET/PET at savanna sites (Williams et al., 2009). The use of climatology to derive this component often suffers in semi-arid climates where variability in vegetation can be high. This is most apparent at the savanna sites, where the GNOAH

HESSD
9, 1547–1587, 2012

model shows a rather smooth annual signal. The introduction of a dynamic component dramatically improves the correlation between observed and modeled LE. The Fisher and GNOAH model use two different satellite sensors (AVHRR and MODIS), and this undoubtedly plays a role in the results as well.

The greatest improvements in modeled LE using the combined model are at the sites with dense vegetation classes. The predictability of LE for the various vegetation using the combined model can be attributed in part to light and water limitation (Mu et al., 2007b). Dense vegetation in the wet tropics is light limited because soil is sufficiently wetted throughout the year, so one would expect that LE is driven primarily by R_N (Priestley-Taylor formulation for PET). Sparse vegetation in the dry tropics on the other hand is water limited (humidity driven), because light is sufficient to maximize stomatal conductance throughout the year and plants close their stomata in response to dry conditions to conserve water and avoid stress. The poor performance of GLDAS R_N and q at the dry and wet sites respectively further augments this relationship.

The use of GNOAH wet canopy evaporation (results not shown) improves correlation with and reduces the RMSE in observed data, though not as significantly as soil evaporation, reflecting its lower importance to total AET. The greatest improvement is seen at the humid site (CG-Euc), which is a challenging region to model, albeit less representative of land-cover in sub-Saharan Africa. The modest improvements can be attributed to the substitution of poor GLDAS specific humidity data and poor parameterization of LE_S with an improved LE_S parameterization driven by a more reliable input variable (precipitation). The small improvements made at the drier sites using the combined model are more difficult to justify, because GLDAS showed higher correlations with observed relative humidity and the performance of the Fisher LE_S component is relatively better at these sites. Erroneous GLDAS R_N appear to be a culprit at the drier sites, but the insensitivity of LE to changes in PET formulization and lower sensitivity of the Berkeley model to R_N, suggest that the use of GNOAH LE_S may make some limited contribution. Although the model is less sensitive to pressure, erroneous values can lead to a 16 % difference between the Fisher and the combined model. This is most

HESSD
9, 1547–1587, 2012

apparent in 2000 at ZA-Kru, where pressure values from the GDAS fields were several kPA higher than for other years.

Improvements in GLDAS specific humidity and pressure fields will undoubtedly reduce the variability in future studies that use the Berkeley model driven by surface reanalysis. Vapor pressure could be used, for example, from a study that recently determined it from MODIS estimates of dew-point temperature in Korea (Ryu et al., 2008). In the meantime, formulations for f_{WET} and f_{SM} involving more certain surface reanalysis inputs than specific humidity/pressure or precipitation, such as maximum and minimum daily surface temperatures, could be used as a substitute. Idso et al. (1975) and more recently Wang et al. (2007) have suggested that the diurnal temperature range is a good indicator of soil moisture status. Under moderately dry to wet conditions, minimum (nighttime) temperature is highly correlated with observed vapor pressure, while midday temperature is indicative of saturation vapor pressure. A formulation for LE that combines temperature driven soil and canopy components can be a powerful tool at both point and grid cell resolution.

The large discrepancy of the models from peak AET at the driest sites could be due to several factors. Although energy balance closure problems are typically associated with errors in measuring turbulent fluxes, measurement error in R_N remains a possibility. Ramier et al. (2009) and Ardo et al. (2008) report only modest daily average energy balance biases of 14.2 $W m^{-2}$ and 16.8 $W m^{-2}$ for NE-Wam and SD-Dem respectively, which does not account for the model underestimation of peak LE by more than 30 %. Another possibility in LE underestimates at NE-Wam and NE-Waf can be the result of unexpectedly low average daytime net radiation during the wet season that appear to result from large increases in longwave outgoing minus longwave incoming (ΔLW) near sunset. The increase in absolute ΔLW can be attributed to increases in soil moisture (lower sensible heat and longwave outgoing) and cloud cover (increased longwave incoming) that is typical during the wet season (Ramier et al., 2009). These factors could lead to a drop in LE of nearly 17 $W m^{-2}$, assuming a one standard deviation drop in R_N from the sensitivity analysis, which still does not account for the underestimation of

HESSD
9, 1547–1587, 2012

LE. The largest contributor to the underestimation of LE is uncertainty in vegetation dynamics: MODIS resolution data is too coarse to adequately capture the vegetation in the presence of heterogeneous terrain, given the strong dependence of the model on EVI and the sparse vegetation at these sites. Even with gross underestimation of R_N and EVI, the comparison of observed data with the Berkeley model reveals that LE remains difficult to model in semi-arid areas. The primary purpose of this paper is to integrate the existing components of the Berkeley model with an LSM. Therefore specific improvements to Berkeley model LE_C, such as the use of the EVI ratio to formulate f_C as in Mu et al. (2007b), calibration of the S in the GNOAH model for semi-arid regions, or the use of different forcing and parameterization data, should be addressed in future studies to reduce uncertainties in semi-arid regions.

In dry areas, it was expected that the advection term, which is included in the Penman formulation for PET, would improve the hybrid model performance over Priestley-Taylor PET. The Penman PET and its input parameters are not available from GLDAS, so a simplified version of Penman PET described in Allen et al. (1998) was evaluated with no improvement at the drier sites. Priestley-Taylor PET may be better at large (satellite) scales, however, because PET at that scale is driven primarily by the expansion of the convective boundary layer, which in turn is driven by R_N (Raupach, 2000). Future calibration can therefore include integration of Priestly-Taylor PET into the GNOAH model.

The residual analysis is less revealing than the sensitivity analysis, as the relationship between GLDAS data and model error are inconsistent across stations. This can be due to a number of factors, including strong multi-collinearity which obscures the effects of independent variables, and the inadequate length of many of the time series. Some results of the residual analysis are worth discussion. For ZA-Kru, the longest time series, heteroskedasticity is observed for all the variables except pressure. This is not unexpected given the non-linearity of the model (larger values in the input can lead to greater variability in the errors). The residual analysis for pressure revealed an inconsistency between the first year and the remaining years of the model run,

HESSD
9, 1547–1587, 2012

suggesting that improvements in pressure can be made by refining GLDAS synthesis across datasets. Given the dependence of the Berkeley model on R_N from the literature it was initially suspected that PET could be an important source of model error. The Penman version of PET described in Allen et al. (1998) and the Priestley-Taylor formulation are compared against the model residuals and no significant relationship are observed for either. This further corroborates the relatively lower sensitivity of the Berkeley model to R_N than vegetation in tropics.

It is difficult to make a more detailed assessment on the performance of the combined model, however, because the comparison is done using point data scaled up to moderate and coarse data. Ideally, the satellite and surface reanalysis scale data should capture the average of a grid cell corresponding to the station used for validation. This assumption is problematic and scaling flux tower data to coarser scales therefore remains an active area of research. The greatest challenge is finding flux towers that lie within homogenous and flat terrain corresponding to the spatial resolution of satellite or surface reanalysis data. If the fetch of the flux tower includes heterogeneous and/or rough terrain, eddy formation can be highly variable and may not be consistent with the areal average (Baldocchi et al., 1988). A possible solution can be to evaluate these models using several flux towers within a grid cell, representing the various land cover types and taking a weighted average to compare with coarser scale data. Another difficulty arises in the nature of the input variables. Many input variables, such as NDVI, scale non-linearly (McCabe and Wood, 2006). Coarser scale inputs capture regional estimates of ET well, so the model can be further validated using larger scale surrogates of ET. For example, the combined model is recently used to develop a crop stress index that successfully tracked multi-year district-level crop yield and identified historical food insecure hotspots in Kenya (Marshall et al., 2011a). Runoff data, which can be used with precipitation to validate the model using a water balance approach, is extremely limited after the year 2000 for basins in sub-Saharan Africa. These data are being used to evaluate the model in a future study which extends the ET time series back to 1981 (Marshall et al., 2011b).

HESSD
9, 1547–1587, 2012

The quantity and quality of field data remains an important obstacle in developing an AET model for sub-Saharan Africa. Several sites that are part of CarboAfrica and AMMA have not undergone any rigorous pre-processing. CG-Tch, for example, had frequent failures with the sonic anemometer between December 2006 and July 2007, which contributed to a lower monthly average, likely reflecting the models' inability to capture the peak LE at this time. Other stations which can help to calibrate and validate AET models for other landcover classes and over larger areas are just coming online. AMMA, for example, has deployed a network of stations in West Africa. At least one of the sites has been scaled to grid resolution using readings from multiple locations within the grid and land cover fractions. At the time this paper is written, the data from those stations included all of the necessary inputs to run the Berkeley model, but did not include LE necessary for model evaluation. In the next few years, when stations have been online long enough, the process of model development should be revisited.

5 Conclusions

The need to understand energy and water fluxes in data sparse regions of the world is an important field of research that demands the use of cost-effective and efficient modeling approaches. In this paper, a new approach to modeling AET, an important energy and moisture flux, has been introduced. For the first time, an AET model has been evaluated using the eddy covariance technique over areas representing major land-cover classes in sub-Saharan Africa. The paper highlights many of the obstacles and limitations of such an analysis. Even with these shortcomings, a model, which combines LE components driven by remote sensing vegetation and precipitation re-analysis has been developed that provides better AET estimates than the individual models. Perhaps the most important contribution of this work is the assessment of the two models across diverse land-cover types and climatic zones. Several potential limitations in each AET model are identified. Namely, these are the use of vegetation climatology to model transpiration in semi-arid regions instead of dynamic vegetation

HESSD
9, 1547–1587, 2012

and the use of specific humidity reanalysis to model soil evaporation in humid areas. R_N reanalysis is of limited use in semi-arid regions, though its contribution to overall model error is less than vegetation and specific humidity. Future work will evaluate the model using historical forcing and test data. This will allow researchers for the first time to make reliable estimates of the surface water budget and to conduct water balance and water resource assessment type studies across sub-Saharan Africa. In the meantime, the current model is being used in conjunction with precipitation indices to enhance crop monitoring in sub-Saharan Africa.

Acknowledgements. This work was primarily supported by the US Agency for International Development through a US Geological Survey cooperative agreement (04HQAG0001) and National Aeronautics and Space Administration Precipitation grant (NNX07AG26G). The eddy covariance data was acquired by the Fluxnet community via the financial support of CarboEuropeIP, FAO-GTOS-TCO, iLEAPS, Max Planck Institute for Biogeochemistry, National Science Foundation, University of Tuscia, Université Laval and Environment Canada and US Department of Energy and the database development and technical support from Berkeley Water Center, Lawrence Berkeley National Laboratory, Microsoft Research eScience, Oak Ridge National Laboratory, University of California – Berkeley, University of Virginia. The authors would also like to acknowledge the contribution of eddy covariance data through AMMA, which is based on a French initiative to build an international scientific group, and was funded by a large number of agencies, especially from France, the UK, the US and Africa, as well as by the European Community's Sixth Framework Research Programme.

References

Allen, R. G., Pereira, L. S., Raes, D., and Smith, M.: Crop evapotranspiration – Guidelines for computing crop water requirements , Food and Agriculture Organization of the United Nations, Rome, Italy, 15 pp., 1998.

Ardo, J., Molder, M., El-Tahir, B. A., and Elkhidir, H. A. M.: Seasonal variation of carbon fluxes in a sparse savanna in semi arid Sudan, Carbon Balance Manage., 3, 18 pp., doi:10.1186/1750-0680-3-7, 2008.

HESSD

9, 1547–1587, 2012

Baldocchi, D. D., Hincks, B. B., and Meyers, T. P.: Measuring Biosphere-Atmosphere Exchanges of Biologically Related Gases with Micrometeorological Methods, Ecology, 69, 1331–1340, 1988.

Betts, A. K., Chen, F., Mitchell, K. E., and Janjic, Z. I.: Assessment of the Land Surface and Boundary Layer Models in Two Operational Versions of the NCEP Eta Model Using FIFE Data, Mon. Weather Rev., 125, 2896–2916, 1997.

Boni, G., Entekhabi, D., and Castelli, F.: Land Data Assimilation with Satellite Measurements for The Estimation of Surface Energy Balance Components and Surface Control on Evaporation, Water Resour. Res., 37, 1713–1722, 2001.

Boone, A., Decharme, B., Guichard, F., Rosnay, P., Balsamo, G., Beljaars, A., Chopin, F., Orgeval, T., Polcher, J., Delire, C., Ducharne, A., Gascoin, S., Grippa, M., Jarlan, L., Kergoat, L., Mougin, E., Gusev, Y., Nasonova, O., Harris, P., Taylor, C., Norgaard, A., Sandholt, I., Ottlé, C., Poccard-Leclercq, I., Saux-Picart, S., and Xue, Y.: The AMMA Land Surface Model Intercomparison Project (ALMIP), Bull. Am. Meteorol. Soc., 90, 1865–1880, 2009.

Bouchet, R. J.: Evapotranspiration reelle et potentielle, signification climatique, Int. Assoc. Hydrol. Sci., 62, 134–142, 1963.

Chen, F. and Dudhia, J.: Coupling an Advanced Land Surface-Hydrology Model with the Penn State-NCAR MM5 Modeling System, Part I: Model Implementation and Sensitivity, Mon. Weather Rev., 129, 569–585, 2001.

Chen, F., Mitchell, K., Schaake, J., Xue, Y., Pan H., Koren, V., Duan, Q. Y., Ek, M., and Betts, A.: Modeling of land surface evaporation by four schemes and comparison with FIFE observations, J. Geophys. Res., 101, 2896–2916, 1996.

Chen, Y., Randerson, J. T., Van der Wer, G. R., Morton, D. C., Mu, M., and Kashibhatla, P. D.: Nitrogen deposition in tropical forests from savanna and deforestation fires, Glob. Change Biol., 16, 2024–2038, 2010.

DehghaniSanij, H., Yamamoto, T., and Rasiah, V.: Assessment of evapotranspiration estimation models for use in semi-arid environments, Agr. Water Manage., 64, 91–106, 2004.

Diak, G. R., Mecikalski, J., Anderson, M., Norman, J., Kustas, W., Torn, R., and Dewolf, R.: Estimating Land Surface Energy Budgets from Space: Review and Current Efforts at the University of Wisconsin-Madison and USDS-ARS, Bull. Am. Meteorol. Soc., 85, 65–78, 2004.

Dirmeyer, P. A., Gao, X., Zhao, M., Guo, Z., Taikan, O., and Naota, H.: GSWP-2: Multimodel Analysis and Implications for Our Perception of the Land Surface, Bull. Am. Meteorol. Soc., 87, 1381–1397, 2006.

HESSD
9, 1547–1587, 2012

Fisher, J. B., Malhi, Y., Bonal, D., Rocha, H. R., De Araújo, A. C., Gamo, M., Goulden, M. L., Hirano, T., Huete, A. R., Kondo, H., Kumagai, T., Loescher, H. W., Miller, S., Nobre, A. D., Nouvellon, Y., Oberbauer, S. F., Panuthai, S., Roupsard, O., Saleska, S., Tanaka, K., Tanaka, N., Tu, K. P., and von Randow, C.: The land-atmosphere water flux in the tropics, Glob. Change Biol., 15, 2694–2714, 2009.

Fisher, J. B., Tu, K. P., and Baldocchi, D. D.: Global estimates of the land-atmosphere water flux based on monthly AVHRR and ISLSCP-II data, validated at 16 FLUXNET sites, Remote Sens. Environ., 112, 901–919, 2008.

Gao, X., Huete, A. R., Ni, W., and Miura, T.: Optical-Biophysical Relationships of Vegetation Spectra without Background Contamination, Remote Sens. Environ., 74, 609–620, 2000.

Glenn, E. P., Huete, A. R., Nagler, P. L., Hirschboeck, K. K., and Brown, P.: Integrating Remote Sensing and Ground Methods to Estimate Evapotranspiration, Critical Rev. Plant Sci., 26, 139–168, 2007.

Gutman, G. and Ignatov, A.: The derivation of the green vegetation fraction from NOAA/AVHRR data for use in numerical weather prediction models, Int. J. Remote Sens., 19, 1533–1543, 1998.

Haan, C. T.: Statistical Methods in Hydrology, Iowa State Press, Ames, IA, 2nd Edn., 496 pp., 2002.

Hartmann, D. L.: Global Physical Climatology, Academic Press, San Diego, 411 pp., 1994.

Henderson-Sellers, A., Pitman, A. J., Love, P. K., Irannejad, P., and Chen, T. H.: The Project for Intercomparison of Land Surface Parameterization Schemes (PILPS): Phases 2 and 3, Bull. Amer. Meteor. Soc., 76, 489–503, 1995.

Hogue, T. S., Mitchell, K., and Emmerich, W.: Evaluation and Transferability of the Noah Land Surface Model in Semiarid Environments, J. Hydrometeorol., 6, 68–84, 2005.

Huete, A., Didan, K., Miura, T., Rodriguez, E. P., Gao, X., and Ferreira, L. G.: Overview of the radiometric and biophysical performance of the MODIS vegetation indices, Remote Sens. Environ., 83, 195–213, 2002.

Idso, S. B., Jackson, R. D., and Reginato, R. J.: Estimating Evaporation: A Technique Adaptable to Remote Sensing, Science, 189, 991–992, 1975.

Jacquemin, B. and Noilhan, J.: Sensitivity study and validation of a land surface parameterization using the HAPEX-MOBILHY data set, Bound.-Lay. Meteorol., 52, 93–134, 1990.

Jarvis, P. G.: The Interpretation of the Variations in Leaf Water Potential and Stomatal Conductance Found in Canopies in the Field, Philosophical Transactions of the Royal Society of

HESSD
9, 1547–1587, 2012

London, Series B, Biological Sciences, 273, 593–610, 1976.
Jiménez, C., Prigent, C., Seneviratne, S. I., McCabe, M. F., Wood, E. F., Rossow, W. B., G. Balsamo, G., Betts, A. K., Dirmeyer, P. A., Fisher, J. B., Jung, M., Kanamitsu, M., Reichle, R. H., Reichstein, M., Rodell, M., Sheffield, J., Tu, K., and Wang, K.: Global intercomparison of 12 land surface heat flux estimates, J. Geophys. Res., 116, 27 pp., doi:201110.1029/2010JD014545, 2011.
June, T., Evans, J. R., and Farquhar, G. D.: A simple new equation for the reversible temperature dependence of photosynthetic electron transport: a study on soybean leaf, Funct. Plant Biol., 31, 275–283, 2004.
Kalma, J. D., McVicar, T. R., and McCabe, M. F.: Estimating Land Surface Evaporation: A Review of Methods Using Remotely Sensed Surface Temperature Data, Surv. Geophys., 29, 421–469, 2008.
Kelliher, F. M., Leuning, R., Raupach, M. R., and Schulze, E.-D.: Maximum conductances for evaporation from global vegetation types, Agr. Forest Meteorol., 73, 1–16, 1995.
Kumar, S. V., Peters-Lidard, C. D., Tian, Y., Houser, P. R., Geiger, J., Olden, S., Lighty, L., Eastman, J. L., Doty, B., Dirmeyer, P., Adams, J., Mitchell, K., Wood, E. F., and Sheffield, J.: Land Information System – An interoperable framework for high resolution land surface modeling, Environ. Model. Software, 21, 1402–1415, 2006.
Leuning, R., Zhang, Y. Q., Rajaud, A., Cleugh, H., and Tu, K.: A simple surface conductance model to estimate regional evaporation using MODIS leaf area index and the Penman-Monteith equation, Water Resourc. Res., 44, W10419, doi:1029/2007WR006562, 2008.
Mahfouf, J. F., and J. Noilhan: Comparative Study of Various Formulations of Evaporations from Bare Soil Using In Situ Data, Journal of Applied Meteorology, 30, 1354-1365.1991
Mahrt, L. and Ek, M.: The Influence of Atmospheric Stability on Potential Evaporation, J. Appl. Meteorol., 23, 222–234, 1984.
Marshall, M.: Agricultural Drought Monitoring in Kenya Using Evapotranspiration Derived from Remote Sensing and Reanalysis Data, in: Remote Sensing of Drought: Innovative Monitoring Approaches, edited by: Anderson, M. and Verdin, J., Taylor and Francis, London, UK, 2010.
McCabe, M. F. and Wood, E. F. : Scale influences on the remote estimation of evapotranspiration using multiple satellite sensors, Remote Sens. Environ., 105, 271–285, 2006.
Mintz, Y. and Serafini, Y. V.: A global monthly climatology of soil moisture and water balance, Clim. Dynam., 8, 13–27, 1992.

HESSD
9, 1547–1587, 2012

Monteith, J. L.: Evaporation and Environment, Symposia of the Society for Experimental Biology, 19, 205–234, 1965.
Mu, Q., Zhao, M., Heinsch, F. A., Liu, M., Tian, H., and Running, S. W.: Evaluating water stress controls on primary production in biogeochemical and remote sensing based models, J. Geophys. Res., 112, G01012, doi:01010.01029/02006JG000179, 2007a.
Mu, Q., Heinsch, F. A., Zhao, M., and Running, S. W.: Development of a global evapotranspiration algorithm based on MODIS and global meteorology data, Remote Sens. Environ., 111, 519–536, 2007b.
Nagler, P. L., Glenn, E. P., Kim, H., Emmerich, W., Scott, R. L., Huxman, T. E., and Huete, A. R.: Relationship between evapotranspiration and precipitation pulses in a semiarid rangeland estimated by moisture flux towers and MODIS vegetation indices, J. Arid Environ., 70, 443–462, 2007.
Nichols, W. E. and Cuenca, R. H.: Evaluation of the Evaporative Fraction for Parameterization of the Surface Energy Balance, Water Resour. Res., 29, 3681–3690, 1993.
Nishida, K., Nemani, R. R., Glassy, J. M., and Running, S. W.: Development of an evapotranspiration index from Aqua/MODIS for monitoring surface moisture status, Geosci. Remote Sens., IEEE Transactions on, 41, 493–501, 2003.
Olioso, A., Chauki, H., Courault, D., and Wigneron, J.-P.: Estimation of Evapotranspiration and Photosynthesis by Assimilation of Remote Sensing Data into SVAT Models, Remote Sens. Environ., 68, 341–356, 1999.
Palmer, A. R. and Yunusa, I. A. M.: Biomass production, evapotranspiration and water use efficiency of arid rangelands in the Northern Cape, South Africa, J. Arid Environ., 11, 1223–1227, 2011.
Pan, H. L. and Mahrt, L.: Interaction between soil hydrology and boundary-layer development, Bound.-Lay. Meteorol., 38, 185–202, 1987.
Papale, D. and Valentini, R.: A new assessment of European forests carbon exchanges by eddy fluxes and artificial neural network spatialization, Glob. Change Biol., 9, 525–535, 2003.
Penman, H. L.: Natural Evaporation from Open Water, Bare Soil and Grass, Proceedings of the Royal Society of London. Series A, Mathematical and Physical Sciences, 193, 120–145, 1948.
Priestley, C. H. B. and Taylor, R. J.: On the Assessment of Surface Heat Flux and Evaporation Using Large-Scale Parameters, Mon. Weather Rev., 100, 81–92, 1972.
Ramier, D., Boulaina, N., Cappelaere, B., Timouk, F., Rabanit, M., Lloyd, C. R., Boubkraoui, S.,

HESSD
9, 1547–1587, 2012

Métayer, F., Luc Descroix, L., and Wawrzyniaka, V.: Towards an understanding of coupled physical and biological processes in the cultivated Sahel – 1. Energy and water, J. Hydrol., 375, 204–216, 2009.
Raupach, M. R.: Equilibrium Evaporation and the Convective Boundary Layer, Bound.-Lay. Meteorol., 96, 107–142, 2000.
Reichstein, M., Falge, E., Baldocchi, D., Papale, D., Aubinet, M., Berbigier, P., Bernhofer, C., Buchmann, N., Gilmanov, T., Granier, A., Grunwald, T., Havrankova, K., Ilvesniemi, H., Janous, D., Knohl, A., Laurila, T., Lohila, A., Loustau, D., Matteucci, G., Meyers, T., Miglietta, F., Ourcival, J.-M., Pumpanen, J., Rambal, S., Rotenberg, E., Sanz, A., Tenhunen, J., Seufert, G., Vaccari, F., Vesala, T., Yakir, D., and Valentini, R.: On the separation of net ecosystem exchange into assimilation and ecosystem respiration: review and improved algorithm, Glob. Change Biol., 11, 1424–1439, 2005.
Rodell, M., Houser, P. R., Jambor, U., Gottschalck, J., Mitchell, K., Meng, C. J., Arsenault, K., Cosgrove, B., Radakovich, J., Bosilovich, M., Entin, J. K., Walker, J. P., Lohmann, D., and Toll, D. : The Global Land Data Assimilation System, Bull. Am. Meteorol. Soc., 85, 381–394, 2004.
Rosero, E., Yang, Z.-L., Gulden, L. E., and Niu, G.-Y.: Evaluating Enhanced Hydrological Representations in Noah LSM over Transition Zones: Implications for Model Development, J. Hydrometeorol., 10, 600–622, 2009.
Ryu, Y., Kang, S., Moon, S.-K. and Kim, J.: Evaluation of land surface radiation balance derived from moderate resolution imaging spectroradiometer (MODIS) over complex terrain and heterogeneous landscape on clear sky days, Agr. Forest Meteorol., 148, 1538–1552, 2008.
Sellers, P. J.: Canopy reflectance, photosynthesis, and transpiration, II, The role of biophysics in the linearity of their interdependence, Remote Sens. Environ., 21, 143–183, 1987.
Stone, L. R. and Horton, M. L.: Estimating Evapotranspiration Using Canopy Temperatures: Field Evaluation, Agronomy J., 66, 450–454, 1974.
Swets, D. L., Reed, B. C., Rowland, J. D., and Marko, S. E.: A weighted least-squares approach to temporal smoothing of NDVI, in ASPRS Annual Conference, From Image to Information, edited, American Society for Photogrammetry and Remote Sensing, Portland, Oregon, 1999.
Wang, K., Wang, P., Li, Z., Cribb, M., and Sparrow, M.: A simple method to estimate actual evapotranspiration from a combination of net radiation, vegetation index, and temperature, J. Geophys. Res., 112, 15107–15114, 2007.

HESSD
9, 1547–1587, 2012

Williams, C., Hanan, N., Scholes, R. J., and Kutsch, W.: Complexity in water and carbon dioxide fluxes following rain pulses in an African savanna, Oecologia, 161, 469–480, 2009.
Wilson, K., Goldstein, A., Falge, E., Aubinet, M., Baldocchi, D., Berbigier, P., Bernhofer, C., Ceulemans, R., Dolman, H., Field, C., Grelle, A., Ibrom, A., Law, B.E., Kowalski, A., Meyers, T., Moncrieff, J., Monson, R., Oechel, W., Tenhunen, J., Valentini, R., and Verma, S. : Energy balance closure at FLUXNET sites, Agr. Forest Meteorol., 113, 223–243, 2002.
Zeng, N.: Drought in the Sahel, Science, 302, 999–1000, 2003.
Zeng, N. and Neelin, J. D.: The Role of Vegetation-Climate Interaction and Interannual Variability in Shaping the African Savanna, J. Climate, 13, 2665–2670, 2000.

HESSD
9, 1547–1587, 2012

Table 1. Model parameters and equations for the Berkeley Model, where $\lambda = T_{OPT}$, $m_1 = 1.2$, $m_2 = 1.2$, $b_2 = -0.05$, and $\beta = 1.0$.

Parameter	Description	Equation
f_c	Fractional total vegetation cover	f_{IPAR}
f_g	Green canopy fraction	f_{APAR}/f_{IPAR}
f_T	Plant temperature constraint	$e^{-(\frac{T_{max}-T_{opt}}{\lambda})^2}$
f_M	Plant moisture constraint	$f_{APAR}/f_{APAR,MAX}$
f_{APAR}	Fraction of PAR absorbed by green vegetation cover	m_1EVI
f_{IPAR}	Fraction of PAR intercepted by total vegetation cover	m_2 NDVI + b_2
f_{SM}	Soil moisture constraint	$RH^{VPD/\beta}$
f_{wet}	Relative surface wetness	RH^{10}
Topt	Optimum plant growth temperature	T_{MAX} @ max{PAR × f_{APAR} × T_{MAX}/VPD}

HESSD
9, 1547–1587, 2012

Table 2. Model parameters and equations for the Noah Model, where k is Beer's Law extinction coefficient, LAI is the leaf area index, r is the atmospheric resistance, $R_C$is the stomatal resistance, C_h is the surface exchange coefficient for heat and moisture, Θ_1 is the soil moisture in the top soil layer at a given timestep, Θ_W is the wilting point, Θ_{REF} is the field capacity, and f is a scaling constant typically equal to 1 or 2. The change in water holding capacity is defined by P (precipitation), D (drainage) and LE_C (in mass units).

Parameter	Description	Equation
f_C	Fractional total vegetation cover	$e^{-(k_{LAI})}$
B_C	Plant coefficient	$B_C = \frac{r+\Delta}{r(1+C_h R_c)+\Delta}$
β	Soil moisture availability	$(\frac{\Theta 1-\Theta_w}{\Theta_{REF}-\Theta_w})^f$
W_C	Water holding capacity	$f_C P - D - LE_C$
S	Maximum water holding capacity	Optimized constant

HESSD
9, 1547–1587, 2012

Table 3. Eight micrometeorological stations throughout sub-Saharan Africa. Ecosystems are identified with the IGBP convention: croplands/natural vegetation mosaic (CRO), evergreen broadleaf forest (EBF), open shrublands (OSH), savanna (SAV), and woody savanna (WSA). P and T_A are the annual total precipitation and average air temperature respectively.

ID	Name	Country	Latitude	Longitude	Period	IGBP	P (mm)	T_A (°C)	Source
BW-Ma1	Maun-Mopane Woodland	Botswana	19.93° S	23.57° E	2000–2001	WSA	464	22.0	Fluxnet
CG-Euc	Kissoko Eucalyptus Plantation	Congo	4.79° S	11.98° E	2004–2006	EBF	1274	23.5	CarboAfrica
CG-Tch	Tchizalamou	Congo	4.29° S	11.66° E	2006–2008	SAV	1150	25.7	CarboAfrica
NE-WaF	Wankama Fallow	Niger	13.65° N	2.63° E	2006	CRO	519	28.5	AMMA
NE-WaM	Wankama Millet	Niger	13.64° N	2.63° E	2006	CRO	519	28.5	AMMA
SD-Dem	Demokeya	Sudan	13.28° N	30.48° E	2005–2008	SAV	320	26.0	CarboAfrica
ZA-Kru	Skukuza	South Africa	25.02° S	31.50° E	2000–2008	SAV	547	21.9	CarboAfrica
ZM-Mon	Mongu	Zambia	15.44° S	23.25° E	2007–2008	DBF	945	25.0	CarboAfrica

HESSD
9, 1547–1587, 2012

Table 4. Summary statistics of Berkeley model inputs from field data versus Noah reanalysis data. B_1 and B_0 are the slope and intercept of the linear fit and N is the number of monthly samples. The statistics for Noah pressure and specific humidity were derived using relative humidity from the field.

Station ID	R_N (W m^{-2})	T (°C)	q (kg kg^{-1})	p (kPa)
BW-Ma1 ($N = 23$)				
R	0.06	0.85	0.50	−0.11
B_1	0.10	0.96	0.02	−0.33
B_0	211.78	0.19	0.0067	91.17
RMSE	88.71	2.20		
CG-Euc ($N = 30$)				
R	0.72	0.72	−0.46	0.52
B_1	0.23	0.62	−0.04	4.02
B_0	169.17	11.24	0.04	97.92
RMSE	42.99	1.61		
NE-Waf ($N = 12$)				
R	−0.38	0.97	0.94	0.29
B_1	−0.18	1.07	0.03	0.26
B_0	276.28	−0.90	0.002	98.23
RMSE	81.80	1.98		
NE-Wam ($N = 11$)				
R	−0.17	0.93	0.98	0.27
B_1	0.0012	1.13	0.03	0.23
B_0	243.81	−2.28	0.0013	98.12
RMSE	109.52	2.71		
ZA-Kru ($N = 44$)				
R	0.88	0.70	0.71	0.06
B_1	1.29	0.44	0.02	−0.58
B_0	83.43	13.94	0.0029	97.11
RMSE	118.46	2.33		

HESSD
9, 1547–1587, 2012

Table 5. The slope (B_1) and intercept (B_0) of a linear fit of modeled LE using the mean for all input data and 10 000 perturbations of one test input variable (i) versus the test input variable in standard space.

i	B_1 (W m^{-2})	B_0 (W m^{-2})
EVI	29.61	92.61
NDVI	−9.88	74.63
R_N (W m^{-2})	16.77	74.63
p (kPa)	0.73	78.78
q (kg kg^{-1})	24.65	85.81
T (°C)	−16.18	78.78

HESSD
9, 1547–1587, 2012

Table 6. Summary results from the comparison of observed monthly LE to the Fisher, Noah, and hybrid (Fisher LE_C + Noah $LE_{(I,S)}$).

Station ID	Fisher	Noah	Hybrid
BW-Ma1			
R^2	0.70	0.75	0.76
RMSE	30.03	23.58	22.06
% error	32.23	27.79	24.99
CG-Euc			
R^2	0.53	0.71	0.80
RMSE	42.15	67.89	25.31
% error	29.85	53.10	16.44
CG-Tch			
R^2	0.34	0.39	0.38
RMSE	101.34	29.13	65.27
% error	163.85	40.25	92.82
NE-Waf			
R^2	0.82	0.91	0.91
RMSE	85.71	94.97	74.38
% error	67.82	71.20	56.02
SD-Dem			
R^2	0.55	0.53	0.60
RMSE	58.69	67.93	51.56
% error	54.84	65.86	45.00
ZA-Kru			
R^2	0.44	0.45	0.55
RMSE	48.40	34.80	36.00
% error	87.70	59.80	56.67

HESSD
9, 1547–1587, 2012

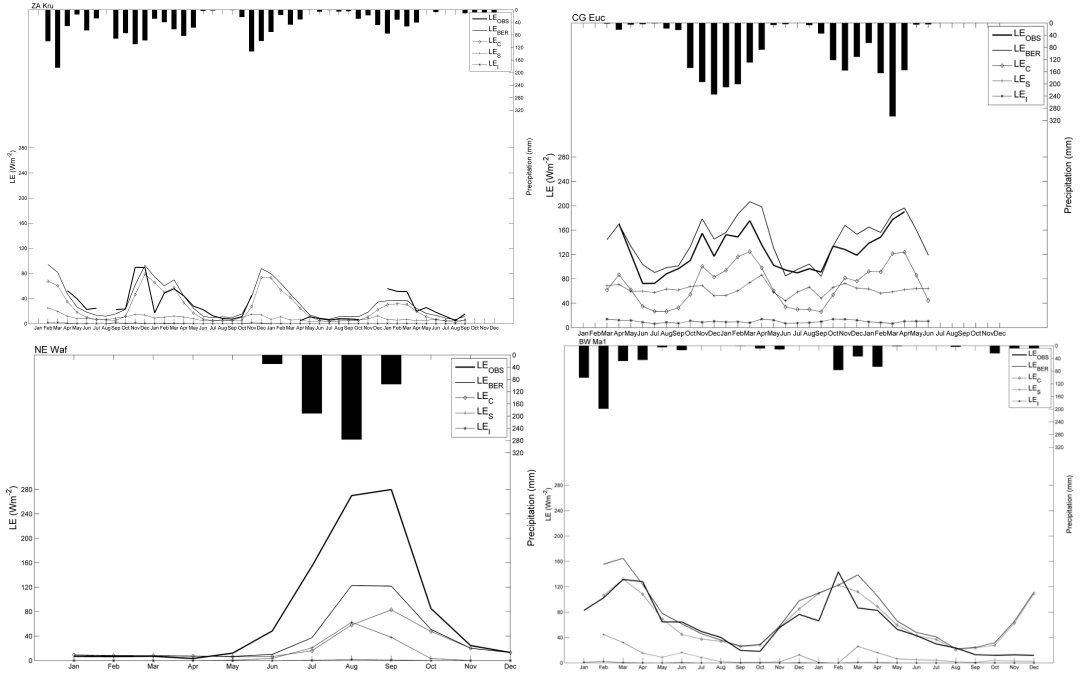

Fig. 1. Monthly observed LE_{OBS} ($W\,m^{-2}$) and modeled LE_{BER} ($W\,m^{-2}$) plotted on the bottom axis and precipitation (mm) plotted on the top axis using field data from ZA-Kru 2000–2003 **(a)**, CG-Euc 2004–2006 **(b)**, NE-Waf 2006 **(c)**, and BW-Ma1 2000–2001 **(d)**.

HESSD
9, 1547–1587, 2012

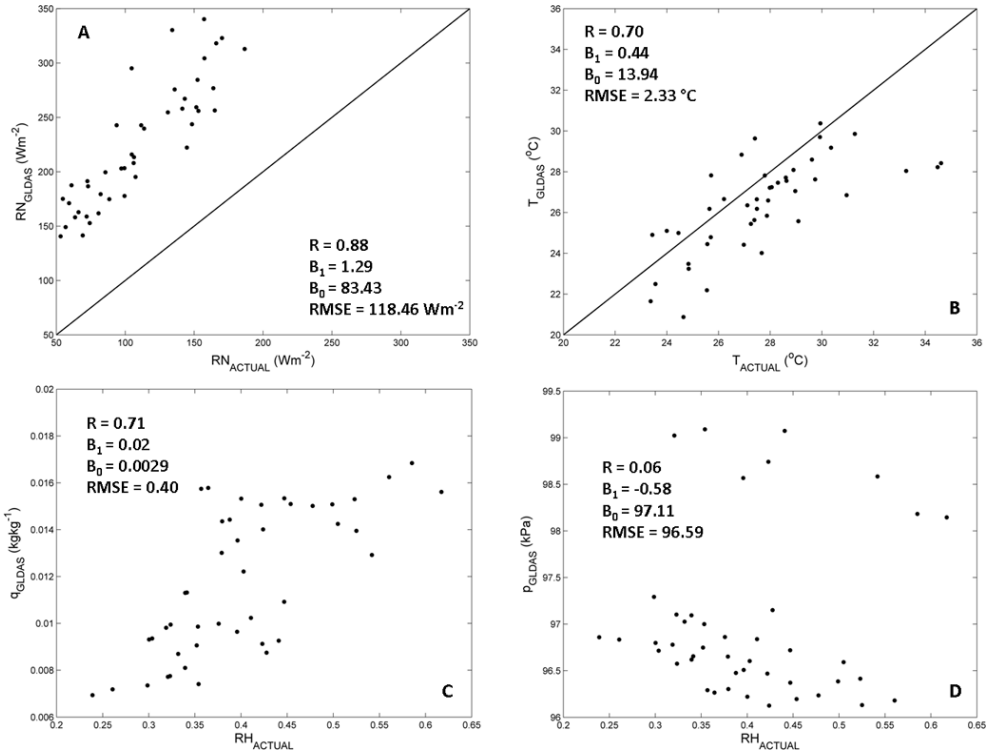

Fig. 2. Plot of Berkeley model inputs from monthly field data versus Noah reanalysis data for ZA-Kru. Net radiation **(a)**, maximum daily temperature **(b)**, specific humidity **(c)**, and surface pressure **(d)**.

HESSD
9, 1547–1587, 2012

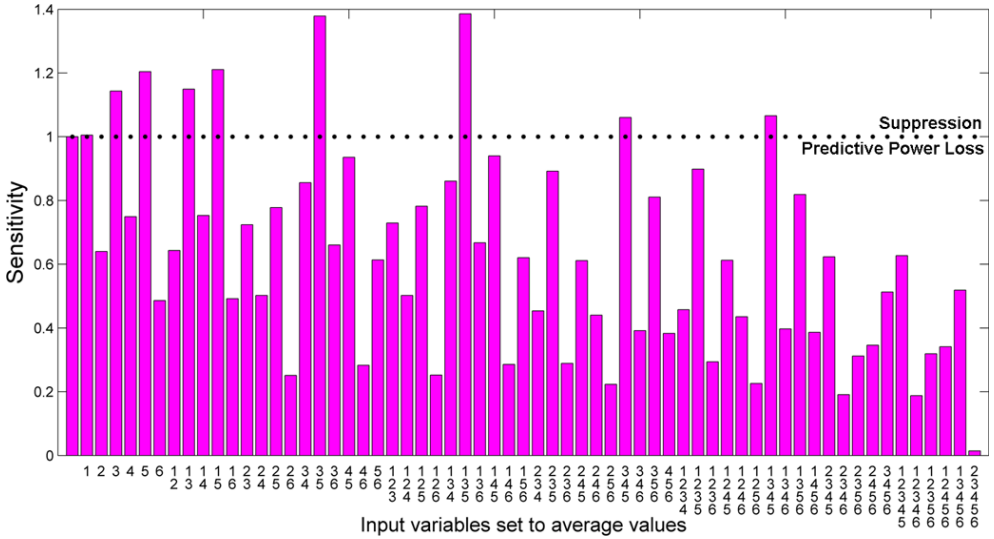

Fig. 3. Conditional case of the sensitivity analysis. The model was run with input variables kept at their average values. Sensitivity on the y-axis is defined as the ratio of the standard deviation of modeled LE with input(s) at their average value to the standard deviation of modeled LE for all possible combinations of input variables. Ratios equal to one, indicate no change from the unconstrained model (leftmost bar graph), while ratios less than one indicate a reduction in predictive power and ratios greater than one indicate damping effects. The input variables are numbered: p (1), q (2), T (3), R_N (4), NDVI (5), and EVI (6).

HESSD
9, 1547–1587, 2012

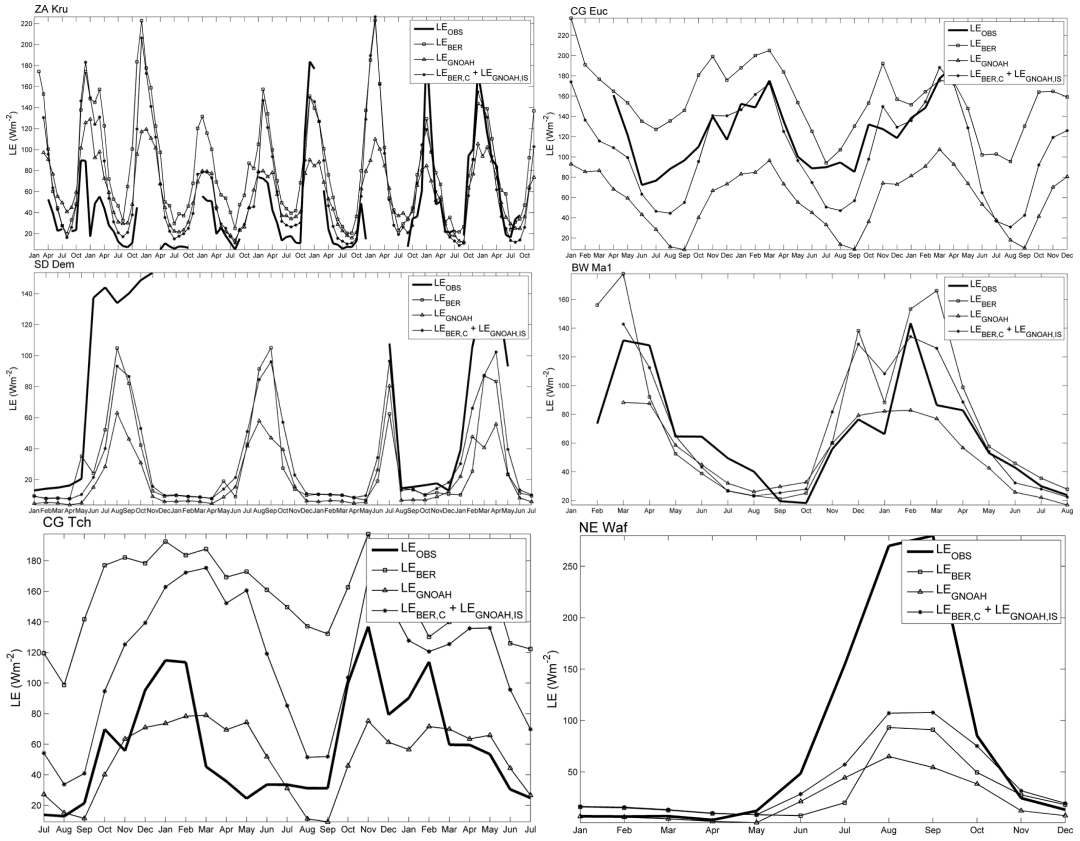

Fig. 4. Monthly time series of available LE data (–) plotted with Fisher LE: Noah LE (Δ), and Fisher LE_C + Noah $LE_{(I,S)}$ (*) for ZA-Kru, CG-Euc, BW-Ma1, SD-Dem, CG-Tch, and NE-Waf.

HESSD
9, 1547–1587, 2012